

# Lateral manipulation of atomic size defects on the $\text{CaF}_2(111)$ surface

S Hirth, F Ostendorf and M Reichling<sup>1</sup>

Fachbereich Physik, Universität Osnabrück, BarbarasträÙe 7, 49076 Osnabrück, Germany

E-mail: [reichling@uos.de](mailto:reichling@uos.de)

Received 8 November 2005, in final form 17 February 2006

Published 10 March 2006

Online at [stacks.iop.org/Nano/17/S148](http://stacks.iop.org/Nano/17/S148)

## Abstract

Atomic scale manipulation on insulating surfaces is one of the great challenges of non-contact atomic force microscopy. Here we demonstrate lateral manipulation of defects occupying single ionic sites on a calcium fluoride (111)-surface. Defects stem from the interaction of the residual gas with the surface. The process of surface degradation is briefly discussed. Manipulation is performed over a wide range of path lengths ranging from tens of nanometres down to a few lattice constants. We introduce a simple manipulation protocol based on line-by-line scanning of a surface region containing defects to be manipulated, and record tip–surface distance and cantilever resonance frequency detuning as a function of the manipulation pathway in real time. We suggest a hopping model to describe manipulation where the tip–defect interaction is governed by repulsive forces.

(Some figures in this article are in colour only in the electronic version)

## 1. Introduction

Manipulation of atomic [1] and molecular [2] species on metal surfaces with the scanning tunnelling microscope (STM) is a well established method offering the possibility of bond formation and rupture [3, 4] conformational change [5] and lateral manipulation [6]. Lateral manipulation is defined as a process of deliberate movement of adsorbates on a surface where the adsorbate never loses contact with the surface [7]; the process is always governed by forces between the tip and adsorbate. In STM experiments, the force is controlled indirectly by the distance between the tip and adsorbate, a quantity that is derived from the tunnelling conductance [8]. Especially for repulsive interactions, the magnitude of the force cannot be related to this parameter because the adsorbate always moves in front of the tip avoiding direct tunnelling. The scanning force microscope (SFM), on the other hand, allows direct measurement and control of both attractive and repulsive forces. STM lateral manipulation experiments are mostly performed at low temperature and only very few room temperature experiments have been reported in the literature [9]. Successful lateral manipulation with the dynamic scanning force microscope has been demonstrated

for germanium [10] and silicon adatoms [11] and tin in a surface alloy with silicon [12]. However, the force controlled manipulation of atomic size species on an insulator surface remains a major challenge and has been attacked only very recently [13]. Here we demonstrate the force controlled manipulation of atomic size defects on a  $\text{CaF}_2(111)$  surface by a raster scanning motion of the tip over a specific surface region containing defects. All measurements reported here were performed at room temperature. Manipulation is facilitated by repulsive forces exerted by moving the tip very close towards the defects. We focus mainly on the presentation of manipulation results and discuss certain circumstances that allow control of the manipulation process and that make it possible to reach every desired position on the surface with the defect. A detailed interpretation of contrast formation, of the manipulation pathway, and details of the interaction mechanisms are left to further studies.

## 2. Experimental procedures

Experiments were performed in a UHV chamber operated at a base pressure below  $1.3 \times 10^{-8}$  Pa. The system was equipped with a commercial dynamic scanning force microscope, namely the UHV 350 from RHK (Troy, Michigan,

<sup>1</sup> Author to whom any correspondence should be addressed.

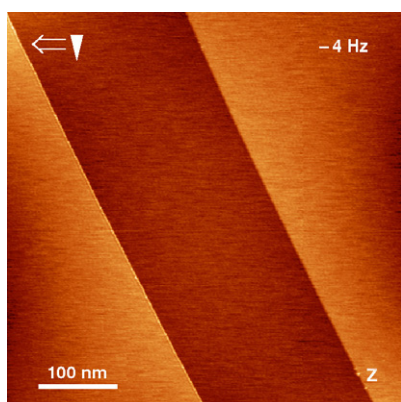


**Figure 1.** Topography image of a freshly cleaved CaF<sub>2</sub>(111) surface showing two steps with a height of one triple layer (315 pm).

USA) providing highest resolution and stability for imaging and manipulation. Procedures for sample preparation and atomic resolution imaging were similar to those used in our previous studies of the CaF<sub>2</sub>(111) surface [14, 15]. The crystal was kept at room temperature during all of the experiments. For imaging and manipulation, we used commercial, uncoated, conductive silicon cantilevers with resonance frequencies of 60–70 kHz and spring constants of a few N m<sup>-1</sup>. *Q*-values were above 80 000 in the UHV. The cantilever oscillation amplitude was kept constant at a level of 18–25 nm. All tips can be assumed to be covered with a native silicon oxide layer when purchased. We used these tips without further treatment such as sputtering or flashing; only a bakeout at 120 °C overnight was performed. For the best imaging contrast, the contact potential was minimized by the application of a typical sample bias voltage of +0.6 V. The contact potential was determined via Kelvin probe force spectroscopy ( $U_{\text{mod}} = 100$  mV).

All of the measurements were performed with the SFM operating in the dynamic frequency detection mode and atomic resolution imaging was accomplished at a typical cantilever resonance frequency detuning of  $-20$  Hz. The topography feedback was set to a very large time constant (1.5 s). Although the feedback was slow compared to the line acquisition time, we could readily pick up topography information except in cases of very fast scanning. Images were taken at a scan speed of 300 ms/line unless stated otherwise.

When manipulating defects, we followed a protocol based on regular line-by-line scanning of the surface as used for imaging. For manipulating defects present in a certain area, the respective region was raster-scanned with the detuning typically increased to  $-35$  Hz. Successful manipulation appeared in the resulting high contrast images as a chain-like manipulation path with an overall direction that is not related to the scanning direction in a simple way. When the desired position was achieved, the tip was retracted from the surface by reducing the detuning to  $-20$  Hz or even lower values. Under the latter conditions, the defect was not manipulated but could be imaged without perturbation. A variation of the manipulation direction was achieved by a change of scanning direction or scanning velocity as will be demonstrated below.

The CaF<sub>2</sub>(111) sample with a size of  $2 \times 3 \times 10$  mm<sup>3</sup> (Korth Kristalle GmbH) was prepared by cleavage of a longer rod in UHV at base pressure and room temperature inside the microscope. A successful preparation yields large atomically flat terraces divided by steps having a height of integer multiples of the F–Ca–F triple layer height (315 pm). A typical topography of the freshly cleaved surface is shown in figure 1. Immediately after cleavage, terraces are found to be absolutely clean, and contamination at step edges that could result from trapping of diffusing molecules cannot be detected even in traces. The small bright features mostly apparent along the step edges are due to charges trapped at crystalline defects. The direction of slow scanning is indicated by the solid arrow ( $\blacktriangledown$ ), for example in the upper left corner of figure 1. Fast scanning was performed perpendicular to this direction in alternating lines from left to right ( $\Rightarrow$ ) and right to left ( $\Leftarrow$ ).

The CaF<sub>2</sub>(111) surface is a prototype insulating surface that is well understood in its SFM atomic contrast formation. As sketched in figure 2(a), the (111) surface consists of stacked triple layers with a height of 315 pm. Fluorine forms the first and third layer and the cubic sites are filled by calcium ions that are missing in every second gap row. In previous work we have shown that contrast formation strongly depends on tip polarity [14]. A negatively terminated tip, images calcium ions as bright circular features but the calcium sub-lattice does not provide unambiguous information about surface directions. When imaging with a positively charged tip, a triangular contrast is observed that is formed by a superposition of interactions between fluorine in the first and third row of a triple layer. The corners of the triangle are determined by the low lying fluorine ions as depicted (white triangle) in panel (d)

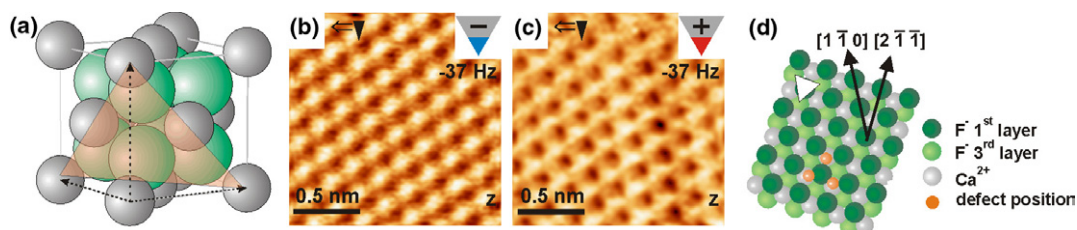


**Figure 2.** Schematic representation and SFM scanning results for the CaF<sub>2</sub>(111) surface. (a) Unit cell of CaF<sub>2</sub>; grey spheres represent calcium and green spheres the fluorine lattice. The (111) plane is shaded in red. Images (b) and (c) demonstrate the two basic contrast patterns found in SFM imaging for negatively and positively terminated nano tips, respectively. Pane (d) shows a model of the (111) surface with an assignment of surface directions as present in images (b) and (c). Dark green spheres represent fluorine in the topmost layer while light green spheres are those at the bottom of the terminating triple layer. The simultaneous imaging of fluorine in those two layers leads to a triangular contrast that is indicated by the white triangle. Grey spheres represent calcium in between fluorine layers. The orange spheres indicate the position of mobile defects.

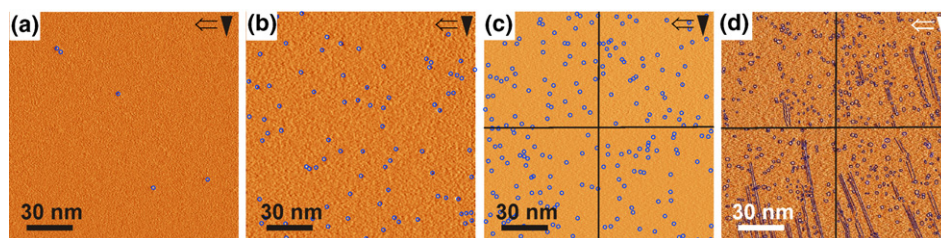


**Figure 3.** Degradation of a  $300 \times 300 \text{ nm}^2$  area on an atomically flat  $\text{CaF}_2(111)$  surface observed in UHV as a function of time. Dark circles mark contaminants on the surface, a few resulting from the preparation but most of them developing during exposure to the residual gas. The black lines in frames (c) and (d) mark the boundaries of the four smaller images that were assembled to form the larger frame. Frame (a) shows the surface directly after cleavage, frame (b) an increased density of impurities after three days. In frame (c) the contamination level is further increased after the 5th day. Frame (d) shows a high density of impurities as observed on the 9th day after cleavage. The quasi-parallel lines indicate manipulation of mobile defects over distances of several tens of nanometres.

of figure 2. This ability of the SFM to image both fluorine sublattices allows an unambiguous identification of all directions in the surface plane. SFM images demonstrating results for both tip terminations shown in panels (b) and (c) were taken on the crystal used for the manipulation experiments. From these images we can deduce the crystal orientation that is the same for all images shown in this report. Therefore, we have an absolute coordinate system for the description of the different manipulation pathways on the surface.

### 3. Results

#### 3.1. Defect preparation

It is well known from SFM imaging experiments on  $\text{CaF}_2$  crystals cleaved in air and on surfaces dosed with gases after vacuum cleavage, that the (111) surface of  $\text{CaF}_2$  is readily degraded by moisture and oxygen [16]. This leads to the formation of randomly distributed nanometre sized features that protrude from the surface by typically less than 100 pm, i.e. much less than the triple layer step height. When exposing the surface to small amounts of gas, the evolution of single defects can be observed and these defects have been attributed to fluorine substitutional hydroxyl groups resulting from the interaction of oxygen and water with mobile surface point defects [17]. These defects, however, should be stationary, because the movement of the defect needs a large amount of energy as fluorine–calcium bonds had to be regularly broken and re-formed. One would expect that the energy for this movement lies in the range of electron volts. This view is supported by the calculations of Catlow *et al* [18] who found the energy to interchange two fluorine ions in the bulk to amount to 2.29 eV, a value that should not be much smaller for movement in the surface layer.

To prepare the surface for manipulation experiments, we simply expose it to the residual gas of the vacuum system that contains water and carbon monoxide as possibly reactive species. The series of images taken over a total time of 144 h shown in figure 3 provides an overview of the degradation of  $\text{CaF}_2$  under UHV conditions in a frame size of  $300 \text{ nm} \times 300 \text{ nm}$ . Defects emerging with time are marked by dark circles for better visibility; any corrugation seen besides the marked defects, is caused by noise present in these fast scanning experiments. As the residual gas pressure

is kept below  $1.3 \times 10^{-8} \text{ Pa}$  throughout the experiment, the development of defects occurs with a time constant comparable to that found in our previous experiments.

The mobile species occur after a few days of exposure, in addition to a large number of stationary defects. This finding strongly indicates that the residual gas first reacts with vacancies on the surface until these reactive centres are saturated, and afterwards adsorbates are only loosely bound to the surface and can therefore be manipulated.

The perfect  $\text{CaF}_2(111)$  surface has no unpaired electrons or vacant orbitals of f- or d-type as present for transition metal salts and other reactive surfaces. Therefore, it has no ability to assist in the homolytic dissociation of bonds or the adsorption by  $\pi$ -binding, but adsorption of polar species is possible on this strongly ionic surface. Theoretical investigations [19, 20] as well as second harmonic generation [21], and helium scattering experiments [22] indicate that molecular water adsorbs on perfectly flat  $\text{CaF}_2(111)$  surfaces without dissociation. Binding stems from the electrostatic interaction between water oxygen and calcium amounting to a binding energy of 0.64 eV ( $-61.8 \text{ kJ mol}^{-1}$ ) at 50% coverage. Less polar species can be expected to exhibit a lower adsorption energy, and their adsorption is unlikely. As the residual gas is composed of non-polar  $\text{H}_2$ ,  $\text{N}_2$ ,  $\text{CO}$ ,  $\text{CO}_2$  and polar  $\text{H}_2\text{O}$ , the latter is the only one likely to adsorb. A definite identification of stable defects as hydroxide ( $\text{OH}^-$ ) and mobile defects as water ( $\text{H}_2\text{O}$ ) is most difficult and could be accomplished with dynamic force microscopy only in conjunction with extended theoretical investigations predicting the apparent contrast for both species in greatest detail.

Occasionally, very few clusters cover the surface directly after cleavage (figure 3(a)) and frames (b)–(d) show how contamination continuously builds up. The last two frames are assembled from four smaller panes, as scanning larger frames became increasingly difficult with an increasing number of contaminants present. The last image of the series exhibits chain-like features that are first indications of manipulation events. The manipulation paths extend over several tens of nanometres, and we note the preferential direction of manipulation in independently scanned panes. All manipulation paths are essentially parallel. Deviations from the preferential direction are caused by scanner piezo creep as the frames were taken consecutively at different positions

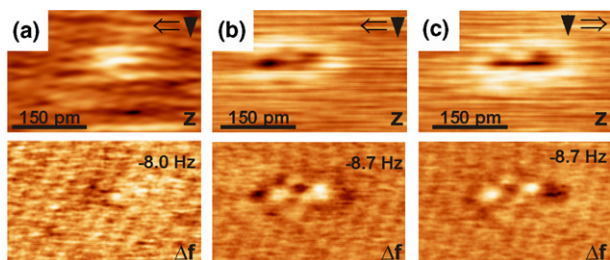


**Figure 4.** Contrast formation studied on a single stationary atomic size defect. Simultaneously recorded topography and detuning images are shown. Frames (b) and (c) have been recorded at an increased detuning compared to frame (a). The increase of 0.7 Hz in detuning results not only in an increased contrast but also a contrast inversion. The apparent elongation of the defect and the characteristic pattern involving dark and bright contrast may be an indication of a repulsive interaction of the foremost tip ions with the defect.

without giving the piezo scanner time to equilibrate after the previous scanning motion.

When scanned at a relatively large tip–surface distance, surface defects appear as protrusions as shown in figure 4(a). However, they change their appearance to that of an indentation when approaching the surface and scanning in a detuning range that resolves individual lattice sites. This predominant contrast is shown in frames (b) and (c) of figure 4 representing the same defect imaged in forward and backward scanning direction, respectively.

A careful analysis of the lattice contrast performed for many images reveals that in most cases imaging is performed with a negatively terminated tip, where the main contrast feature represent calcium ions. Great care was taken to avoid atomic tip changes that would strongly change lattice and defect contrast formation. Manipulation experiments involving strong tip–surface interaction can only be performed in a reproducible manner with exceptionally stable tips.

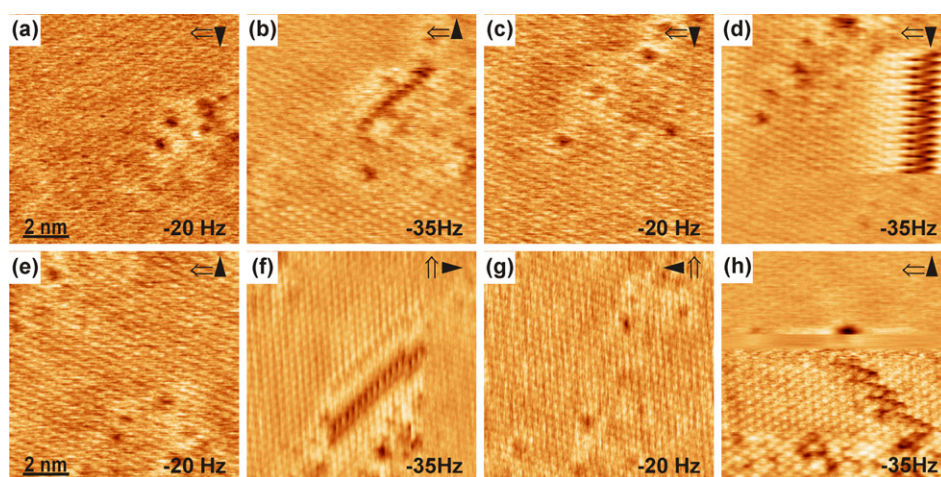


**Figure 5.** Manipulation of a group of defects. Frames (a), (c), (e), and (g) were taken in the imaging mode with an average detuning of  $-20$  Hz. Frames (b), (d), and (f) show manipulation performed with an average detuning of  $-35$  Hz. The chain structure is caused by the repeated imaging of the same defect in the course of the manipulation. The direction of manipulation in frames (b) and (f) is identical despite the interchange of slow and fast scanning direction. The manipulation paths of images (b) and (d) recorded with opposite slow scanning direction enclose an angle of  $120^\circ$ . Manipulation along the third crystal direction was achieved in pane (h). This image was taken on another position on the crystal and is not related to the cycle of panes (a)–(g).

### 3.2. Defect manipulation

The described defects on CaF<sub>2</sub>(111) can be moved by the interaction with the tip, in a fashion demonstrated in figure 5. Frames (a)–(g) are consecutively recorded images that have either been taken in the imaging mode at a detuning of  $-20$  Hz or in the manipulation mode at a detuning of  $-35$  Hz. In this experiment, a group of defects is manipulated on the scale of several nanometres first upwards (frames (a)–(c)) and then downwards (frames (d) and (e)). To explore the dependence of the manipulation direction from the scanning direction, in a last manipulation step the fast and slow scanning directions are interchanged (frames (f) and (g)). As the group is initially close to one side of the imaging frame, defects are partially dispersed and the final pattern of the group of defects is different from the initial one. The strong interaction between tip and defect during scanning in the manipulation mode is apparent in the form of strong contrast features forming lines along the main manipulation direction. The direction of manipulation is not related to the scanning direction in a trivial way in any of the images. We anticipate that the hopping motion from one metastable position to the next one is the origin of the abrupt change in the contrast along the manipulation path.

In this context, it is interesting to investigate the manipulation pathways in frames (b), (d), and (f) of figure 5. These pathways appear as lines enclosing an angle of  $120^\circ$  with each other. This strongly indicates that defects move along specific crystallographic directions on the surface. A similar behaviour is found in STM on noble metal surfaces, where adsorbates are preferentially and more easily manipulated along closed packed directions due to a lower potential surface barrier compared to other crystal directions [23]. It is plausible that this effect is more pronounced on an insulating surface as this surface is composed of positive and negative ions resulting in a surface potential of considerable corrugation [24]. Consequently, we observe movement solely along the high symmetry directions of the crystal surface from one calcium adsorption position to another. This is analogous

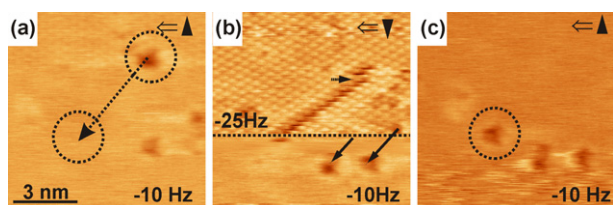


**Figure 6.** Manipulation of a selected defect towards two other defects on the surface. The defect marked by the dotted circle is selected for manipulation over 13 atomic positions along the dotted arrow to the predefined position on the lower left of the frame (marked by dotted circle). The manipulation is shown in frame (b). We observe a glitch of the defect by one atomic spacing to the right, indicated by the horizontal arrow. When the position of the two remaining defects is reached, they are also manipulated (indicated by solid arrows). Because the right defect comes into the proximity of the tip earlier, its manipulation path (2.7 nm) is longer than the path of the left defect (1.7 nm). Frame (c) shows the new configuration of the defect group with the selected defect manipulated to the desired position missed by one lattice spacing (marked by dotted circle).

to STM manipulation, where small adsorbates also will not occupy unfavourable surface sites but stay at the most stable adsorption position. Manipulation curves, therefore, reproduce the periodicity of the underlying substrate [25].

As in the measurement of figure 5, we frequently observe that more than one defect is manipulated, and we assume that this is due to the fact that manipulation is not only performed by the tip terminating cluster providing the atomically resolved image but also by the force field of larger parts of the tip apex. The range of this interaction can be explored by the manipulation shown in figure 6, where a defect in some distance to two other defects is moved downwards, almost to the pre-defined position (frame (b)). The desired final position is missed by one lattice spacing due to a glitch in the wrong direction at the position indicated by the arrow. A refinement of the manipulation protocol is needed to minimize the number of such deviations. When the tip approaches the lower defects by approximately 0.6 nm, they are moved towards the bottom of the scanning area pointing to another peculiarity of this kind of manipulation. An extremely sharp tip is needed to accomplish

manipulation of a single entity closely surrounded by other mobile species.

### 3.3. Contrast formation

For a better understanding of the manipulation images, it is helpful to analyse results from different channels recorded during imaging and manipulation. In figure 7, we compare data obtained by scanning the same surface area. These images show only a fraction of the scanned area. Therefore, the initial position of the defect is not visible in imaging mode frames. Imaging and manipulation frames display the topography ( $z$ ), detuning ( $\Delta f$ ) and energy dissipation ( $\Gamma$ ) signals, respectively. We find that any atomic contrast in  $\Gamma$  is below the noise level for the imaging experiment, however atomic contrast is faintly visible when scanning under manipulation conditions, as well as a slight enhancement above the manipulation path. No further contrast features are visible in the dissipation frame demonstrating the excellent stability of the tip used in these experiments.

Cross-sectional data shown in panes (g)–(i) provide the orders of magnitude for the observed signals taken along the manipulation path drawn in a pale shade for the imaging mode and in black for the manipulation mode. While the corrugation of topography and detuning signals are 2 pm and 1.5 Hz during imaging and increase by a factor of 30 and 3.5 during manipulation, respectively, the corrugation in the dissipation signal increases from noise to a value of 86 meV/cycle.

It is important to note, however, that the presence and strength of the dissipation signal strongly depends on the tip conditions and does most probably not contain any useful information about the manipulation process. Atomic corrugation in the dissipation channel is only very rarely found in manipulation experiments as dissipation is intimately related to tip instability while manipulation is possible only with very stable tips. To illustrate the relation between dissipation and tip instability, in figure 8 we present a comparison of simultaneously recorded detuning and dissipation data taken in the imaging mode on a surface area containing a defect. The main feature here is that the dissipation signals exhibits extremely strong variations within a single frame while the

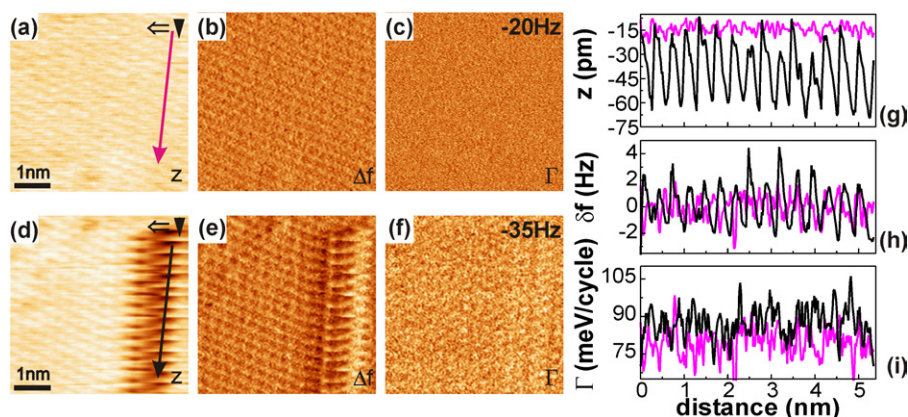


**Figure 7.** Contrast formation in the topography ( $z$ ), detuning ( $\Delta f$ ), and dissipation ( $\Gamma$ ) channels simultaneously recorded on a  $10.2 \text{ nm} \times 10.2 \text{ nm}$  frame scanned in the imaging ((a)–(c)) and manipulation ((d)–(f)) modes, respectively. The profiles on the right are cross-sections taken in the region of defect manipulation along the lines indicated by the pale (imaging mode) and black (manipulation mode) arrows.  $\delta f$  denotes the corrugation in the detuning signal as calculated from the difference between the measured and pre-set detuning  $\delta f = \Delta f - \Delta f_{\text{set}}$ .

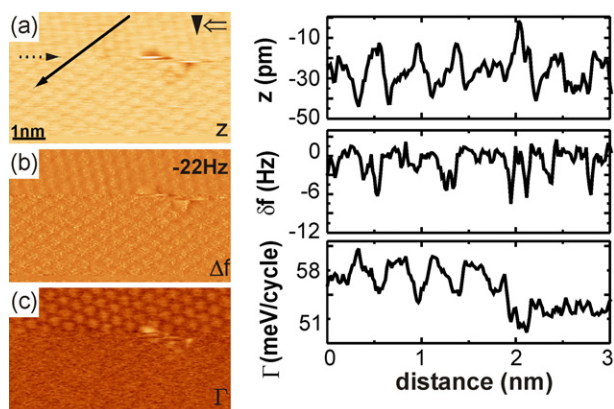


**Figure 8.** Average corrugation of (a) topography ( $z$ ), (b) detuning ( $\Delta f$ ), and (c) dissipation ( $\Gamma$ ) for a  $10.2 \text{ nm} \times 10.2 \text{ nm}$  frame scanned in the imaging mode. In the line marked by the dotted arrow a tip change occurs during the interaction of the tip with a defect, decreasing the mean dissipation from 58 to 52 meV/cycle and removing the atomic corrugation in this channel. The cross-sections shown on the right have been taken along the solid arrow in frame (a).  $\delta f$  denotes the corrugation in the detuning signal as calculated from the difference between the measured and pre-set detuning  $\delta f = \Delta f - \Delta f_{\text{set}}$ .

detuning signal is fairly stable in its magnitude. The interaction of the tip with the defect causes a tip change (see dotted arrow in frame (a)) resulting in the complete loss of the formerly strong dissipation contrast. This is a well known phenomenon in dynamic mode scanning force imaging in cases where dissipation is a result of dynamic instability of parts of the tip that are not mainly involved in the formation of the detuning contrast [26, 27]. A molecule attached to the side of the tip can be subject to weak periodic forces during the oscillatory tip movement without contributing significantly to the detuning contrast. If the movement of the molecule is governed by a potential with two minima and a form that changes during the oscillation cycle, the tip–surface interaction becomes non-conservative and a dissipation signal can be observed [28]. It has, furthermore, been demonstrated by theory that increasing temperature may reduce the level of this type of dissipation by one order of a magnitude because then energy for non-conservative interactions can be provided by the tip oscillation as well as from the heat bath [28]. This could explain why the atomic dissipation is weak or below the noise level of our

highly sensitive instrument for some of our room temperature measurements even if there is some tip instability present.

Although, the detailed tip structure and its instability is not known for our measurements and, therefore, the details of dissipation contrast remain obscure, it is clear from the above discussion that there is no indication that the manipulation process contributes significantly to the generation of the dissipation signal. On the other hand, one would expect significant dissipation if the tip–surface interaction involved the periodic formation and rupture of bonds between the tip and the manipulated entity. We take the absence of manipulation related dissipation signals as a strong indication that the manipulation process is governed by a pushing type of motion resulting from repulsive forces rather than a pulling type of interaction involving at least weak bond formation according to the nomenclature introduced in the context of STM manipulation [29].

### 3.4. Velocity dependence

The direction of manipulation, namely the preferred direction for defect hopping can be influenced by a variation of the scanning speed as is illustrated in figure 9. The manipulation path is shown in frame (a) and (b), while in sketch (c) we marked a series of positions that are occupied during defect movement. At slow scanning speed, the path of the defect appears to be broader than for fast scanning, and hopping occurs more often in the direction of the slow scanning direction for both forward and backward scanning motion. With increased scanning speed, the visible manipulation path becomes more narrow and the manipulation is more directional. By the right choice of the scanning speed, virtually any manipulation direction is accessible, as is indicated by the dotted arrows next to frame (a). Therefore, the method does not only allow the demonstration of simple manipulation events but could principally also be used to perform more sophisticated manoeuvres.

## 4. Summary

While a detailed understanding of the manipulation mechanism requires further efforts in analysis of experiments and theoretical modelling that are beyond the scope of this paper, here we outline a few important points providing a preliminary understanding of the process. The key assumption is that the

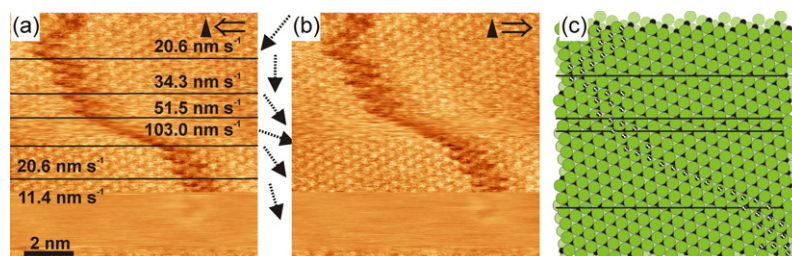


**Figure 9.** Velocity dependence of the manipulation path. (a) A topography image recorded in the manipulation mode where the scanning speed was changed in a systematic manner. (b) The corresponding image for the opposite direction. The images were taken at an average detuning of  $-35 \text{ Hz}$ . To enhance the contrast of the substrate lattice, the raw data was merged with the FFT filtered image of the substrate weighted 25% of the raw data. Black lines separate areas of different scan velocity. The dotted arrows denote the preferential direction of movement as deduced from the resulting image. (c) Schematic representation of the surface with indicators of preferential sites during manipulation.

main interaction resulting in the manipulation is repulsive, and manipulation is facilitated by a series of hopping events during scanning in both directions. When the tip is relatively far away from the defect, repulsion causes a local relaxation in form of an evasion of the defect inside a potential trough associated with a neighbouring lattice ion. Upon approach, the repulsive force becomes increasingly stronger and when exceeding a certain limit, hopping motion occurs from one potential trough to the next neighbour.

Preferred hopping directions are along the calcium ions. With the substrate oriented as indicated in figure 2(d), hopping to neighbouring sites is not equal for all directions. Because of the angle between a symmetry axis of the substrate and the fast scanning direction, it is likely that the potential energy path along the fast scanning direction is not the same for movement to the right and the left, therefore, leading to different probabilities for a hopping event for the two directions. We expect that in further studies we will be able to much more precisely pre-determine the gross direction of the manipulation by a proper choice of the scanning direction with respect to the crystallographic directions. Glitches during manipulation could be avoided by using a more elaborate manipulation protocol as well as improved software.

## Acknowledgments

This work was supported by the single molecules program of the Stiftung Volkswagenwerk and the framework 6 specific targeted research project *NanoMan* of the European Commission. S Hirth gratefully acknowledges support from the Stiftung des Verbandes der deutschen chemischen Industrie. Fruitful discussions with Ó Custance, S Gritschneider, G Meyer, R Nishi, A Kühnle and A L Shluger are most gratefully acknowledged.

## References

- [1] Meyer G, Repp J, Zöphel S, Braun K-F, Hla S W, Fölsch S, Bartels L, Moresco F and Rieder K H 2000 *Single Mol.* **1** 79–86
- [2] Moresco F, Meyer G, Rieder K-H, Tang H, Gourdon A and Joachim C 2001 *Appl. Phys. Lett.* **78** 306–8
- [3] Lee H J and Ho W 1999 *Science* **286** 1719–22
- [4] Hansen A G, Boisen A, Nielsen J U, Wackerbarth H, Chorkendorff I, Andersen J E T, Zhang J and Ulstrup J 2003 *Langmuir* **19** 3419–27
- [5] Moresco F, Meyer G, Rieder K-H, Tang H, Gourdon A and Joachim C 2001 *Phys. Rev. Lett.* **86** 672–5
- [6] Keeling D L, Humphry M J, Moriarty P and Beton P H 2002 *Chem. Phys. Lett.* **366** 300–4
- [7] Moresco F, Meyer G, Tang H, Joachim C and Rieder K H 2003 *J. Electron Spectrosc. Relat. Phenom.* **129** 149–55
- [8] Hla S W and Rieder K H 2003 *Annu. Rev. Phys. Chem.* **54** 307–30
- [9] Li J, Berndt R and Schneider W-D 1996 *Phys. Rev. Lett.* **76** 1888–91
- [10] Oyabu N, Sugimoto Y, Abe M, Custance Ó and Morita S 2005 *Nanotechnology* **16** S112–7
- [11] Oyabu N, Custance Ó, Yi I, Sugawara Y and Morita S 2003 *Phys. Rev. Lett.* **90** 176102
- [12] Sugimoto Y, Abe M, Hirayama S, Oyabu N, Custance Ó and Morita S 2005 *Nat. Mater.* **4** 156–9
- [13] Nishi R, Miyagawa D, Seino Y, Yi I and Morita S 2006 *Nanotechnology* **17** S142–7
- [14] Foster A S, Barth C, Shluger A L and Reichling M 2001 *Phys. Rev. Lett.* **86** 2373–6
- [15] Barth C, Foster A S, Reichling M and Shluger A L 2001 *J. Phys.: Condens. Matter* **13** 2061–79
- [16] Reichling M, Huisinga M, Gogoll S and Barth C 1999 *Surf. Sci.* **439** 181–90
- [17] Reichling M and Barth C 1999 *Phys. Rev. Lett.* **83** 768–71
- [18] Catlow C R A, Norgett M J and Ross T A 1977 *J. Phys. C: Solid State Phys.* **10** 1627–40
- [19] de Leeuw N H, Purton J A, Parker S C, Watson G W and Kresse G 2000 *Surf. Sci.* **452** 9–19
- [20] de Leeuw N H and Cooper T G 2003 *J. Mater. Chem.* **13** 93–101
- [21] Zink J C, Reif J and Matthias E 1992 *Phys. Rev. Lett.* **68** 3595–8
- [22] Lehmann A, König G and Rieder K H 1995 *Chem. Phys. Lett.* **235** 65–8
- [23] Kühnle A, Meyer G, Hla S W and Rieder K-H 2002 *Surf. Sci.* **499** 15–23
- [24] Foster A S, Shluger A L and Nieminen R M 2002 *Appl. Surf. Sci.* **188** 306–18
- [25] Meyer G, Bartels L, Zöphel S and Rieder K H 1999 *Appl. Phys. A* **68** 125–9
- [26] Loppacher C, Bennowitz R, Pfeiffer O, Guggisberg M, Bammerlin M, Schär S, Barwich V, Baratoff A and Meyer E 2000 *Phys. Rev. B* **62** 13674–9
- [27] Loppacher C, Bammerlin M, Guggisberg M, Schär S, Bennowitz R, Baratoff A, Meyer E and Güntherodt H J 2000 *Phys. Rev. B* **62** 16944–9
- [28] Kantorovich L N and Trevethan T 2004 *Phys. Rev. Lett.* **93** 236102
- [29] Bartels L, Meyer G and Rieder K H 1997 *Phys. Rev. Lett.* **79** 697–700